

1
2
3
4
5
6
7
8
9
10
11
12
13
14
15
16
17
18
19
20
21
22
23
24
25

New directional wave satellite observations : Towards improved wave forecasts and climate description in Southern Ocean

L. Aouf¹, D. Hauser², B. Chapron³, A. Toffoli⁴, C. Tourrain⁵, C. Peureux⁶

¹Météo-France, CNRM-DirOP, Toulouse, France

²LATMOS/IPSL, Guyancourt, France

³IFREMER, Brest, France

⁴University of Melbourne, Melbourne, Australia

⁵CNES, Toulouse, France

⁶CLS, Brest, France

Corresponding author: Lotfi Aouf (lotfi.aouf@meteo.fr)

†Current address : Météo-France, DirOP/MAR, 42 Avenue Gaspard Coriolis Toulouse 31057 Cedex 1, France..

Key Points:

- The assimilation of partitions wavenumber components induces a significant reduction of SWH bias in Southern Ocean.
- The study clearly reveals the improvement of the energy transfer of wind waves during the wave growth phase under unlimited fetch conditions such in Pacific Southern Ocean.
- The wave age and dominant wavenumber have been significantly corrected by the assimilation of directional observations of SWIM compared to the assimilation of SWH-nadir only.

26 **Abstract**

27 In spite of continuous improvements of ocean wave models in the last decades, results still show
28 large in certain condition, in particular in strongly forced conditions, as encountered in the
29 Southern Ocean, where strong westerly winds generate some of the fiercest waves on Earth in
30 almost unlimited fetch conditions. The newly launched Chinese-French Oceanography Satellite
31 (CFOSAT) provides directional spectra of ocean waves for both wind seas and swells. Compared
32 to Synthetic Aperture Radar (SAR), it resolves shorter wavelengths, which dominates in non-
33 fully developed wind waves. Here we demonstrate that the assimilation of the wave number
34 components from CFOSAT spectra produce more accurate predictions of wave growth than
35 assimilation of significant wave height alone and results in a notable reduction of model bias in
36 the Southern Ocean, especially in the Pacific Ocean sector. In addition results also indicate a
37 downward shift of the wave age consistent with theoretical wave growth curves.

38

39 **Plain Language Summary**

40

41 This work focuses on the importance of using directional wave observations to improve model
42 wave prediction in the Southern Ocean. The results indicate a significant impact on the transition
43 from a wind-dependent sea to a well-developed sea. A direct consequence of this work will
44 concern a better understanding of the wave climate in Southern Ocean and therefore an
45 improvement of coupled ocean/waves/atmosphere systems.

46

47 **1 Introduction**

48 The accuracy of wave prediction models has increased notably over the past decade, following
49 the improvement of atmospheric models, which provide the wind forcing. Furthermore,
50 development of assimilation techniques has allowed the incorporation of satellite data into
51 models to optimize performances (Lionello et al, 1992). In this respect, space-borne altimeter
52 sensors scan the ocean surface globally and return observations of significant wave height—a
53 measure of the overall energy content of the wavy surface—which contributes to adjusting the
54 variance of the wave energy spectrum. Moreover, Synthetic Aperture Radar (SAR) technology
55 provides images that can be converted into directional wave energy spectra. Assimilation of the
56 latter enables a more comprehensive control of the energy density function, not only allowing the
57 optimization of the variance, but also controlling wave periods and wave directions for example
58 (Aouf et al, 2019). Nevertheless, SAR only detects swell systems, i.e. a long wave system no
59 longer under the effect of local wind, with wavelength longer than 200 m (Collard et al. 2005),
60 but does not resolve, and thus assimilation does not correct, the wind sea, i.e. the short-wave
61 components directly generated by the local wind.

62 Generation and growth of wind sea depend on the fetch conditions (Hasselmann et al, 1973,
63 Donelan et al, 1985, Young 1999), and generate (nonlinear) energy transfer across wave scales
64 until an equilibrium state (full development) is reached. More specifically, the transfer consists
65 of an inverse cascade transferring energy from high to low frequencies, which downshifts the
66 spectral peak, stretches the wavelengths and consequently accelerates the wave phase speed.

67 Growth stops, and wind sea becomes swell, when the ratio of the wave phase speed to the wind
68 speed (i.e. wave age) is greater than about 1.2 (atmosphere cannot force waves that move faster
69 than the wind, Pierson and Moskowitz 1964, Phillips 1977, Hasselmann et al. 1973, Young
70 1999). Concomitantly, there is a direct cascade that shifts energy towards high frequencies,
71 forcing energy to dissipate mostly by wave breaking and counterbalancing wind input.

72 Energy further re-distributes across directions so that the wave spectrum broadens during growth
73 (e.g. Hasselmann et al , 1980, Donelan et al, 1985, Fadaeiazar et al., 2020). The directional
74 distribution and integrated values such as the mean wave direction are crucial parameters
75 affecting wave growth through wind input, as the atmosphere forces energy into wave
76 components that are aligned (and almost aligned) with wind. Despite their role, however,
77 directional properties remain one of the less known properties of the ocean surface.
78 Contemporary wave models use parametrizations to shape the directional spreading during the
79 wave growth, which assume the directional distribution being unimodal (i.e. energy is
80 concentrated around one dominant direction, Hasselmann et al. 1980, Mitsuyasu et al. 1975,
81 Donelan et al. 1985) and defined by a directional spreading function of the form $\cos^{2s}(\vartheta)$, where
82 ϑ is the wave propagation direction. Nevertheless, there is no general consensus on the shape of
83 the directional distribution. Moreover, field and laboratory observations have also suggested that
84 the nonlinear interactions induce a bimodal directional distribution in the early state of wave
85 growth (Young 1995, Ewans 1998, Toffoli et al. 2010, Toffoli et al. 2017), with the angle of
86 separation among peaks depending on the wave age and wind direction (Long and Resio 2006).
87 Peaks eventually merge into a unimodal directional function consistent with $\cos^{2s}(\vartheta)$ when
88 approaching full development (e.g. Toffoli et al. 2017, Fadaeiazar et al., 2020).

89 Uncertainties on the directional properties affect the identification of those wave components
90 that are aligned with the wind and thus translate into errors in the estimation of the wind input
91 process in the wave prediction model. The extent of these errors is yet to be quantified. As
92 contemporary satellite products cannot optimize wind sea, the latter remains a notable source of
93 model errors, resulting in an overestimation of significant wave height (positive bias). This is
94 exacerbated in the Southern Ocean (Ziegler et al. 2015)-a region covering an uninterrupted band
95 of water around Antarctica south of the main landmasses of Africa, Australia, and South
96 America—that is dominated by strong westerly winds, which blows all-the-year-round with
97 almost unlimited fetches and speed in excess of 13 m/s during summer months and 18 m/s during
98 winter months (Young et al. 2020). These intense winds generate some of the fiercest waves on
99 the planet with high percentiles of wave height exceeding 5 m during summer and 7 m during
100 winter (e.g. Babanin et al. 2019, Barbariol et al. 2019, Letraon et al. 2019, Vichi et al. 2019,
101 Young et al. 2020).

102 The newly launched Chinese-French Oceanography Satellite (CFOSAT) uses Surface Wave
103 Investigation Measurements (SWIM) sensor (Hauser et al. 2018) to monitor the ocean surface.
104 Compared to SAR, SWIM resolves a broader range of wavelengths, spanning from 70 to 500 m,
105 and returns a directional wave energy spectrum that includes both wind sea and swells. Here we
106 discuss the effect of data assimilation on model performance in the Southern Ocean. We
107 demonstrate that assimilating directional properties from SWIM spectra improves prediction of
108 energy transfer during wave growth and concurrently of significant wave height. We show that

109 model bias is reduced more efficiently when compared with classical assimilation procedures
110 that incorporate information on the significant wave height only.

111 **2 CFOSAT mission and SWIM spectra**

112 The instrument SWIM of CFOSAT is a real aperture scanning radar which provides directional
113 wave spectra from several off-nadir beams (pointing at 6, 8 and 10°). Each spectrum is
114 representative of an area of about ± 35 km along-track by 90 km on each side of the nadir track,
115 and is discretised over 32 wave numbers from [0.0126–0.279] rad/m, corresponding to the
116 wavelength domain [22–500] m, with a geometric progression of 1.1, and 12 directions, i.e.,
117 every 15° with a 180° ambiguity in the propagation direction. During the calibration/validation
118 phase of the mission a detailed analysis was carried out to evaluate the ability of SWIM to
119 provide accurate parameters from the wave spectra (see Hauser et al. 2020) such as the dominant
120 direction, dominant wave height and significant wave height. It was concluded that, except when
121 waves propagate close to the along-track direction directional wave spectra can be provided with
122 good accuracy over the wavelengths range of 70 to 500 m (see Hauser et al. 2020). In this study
123 we use the directional wave spectra from the beam 10° which have been shown to perform better
124 in comparison with the other beams (see Hauser et al, 2020). SWIM also provides Significant
125 Wave Height (SWH) along its track from nadir measurements just like the classical altimeter
126 measurement (referred to as SWIM-nadir). For the assimilation, we used observations made over
127 a 36 days period from April 26 to 1 June 2019. During this period, 343885 wave spectra from
128 SWIM were collected for the global ocean, and 95281 of which were from the Southern Ocean.

129 **3 Numerical model and data assimilation technique**

130 The MFWAM wave model describes the evolution of wave spectra in space and time
131 through the wave action conservation equation with source terms representing the wave
132 generation by the wind, the non-linear interactions and the wave breaking at sea surface. The
133 wave model MFWAM of Meteo-France is based on the IFS-ECWAM computing code of the
134 ECMWF (see IFS-38R2). The model MFWAM uses an ST4 dissipation term related to wave
135 breaking as developed by Ardhuin et al. (2010). Also, in the MFWAM model the wind input
136 source term takes into account a dissipation term due to the damping of the swell by the surface
137 friction. The non-linear interactions are represented by the Discrete Interaction Approximation
138 (DIA) which is a common approximation in numerical wave models due to its computational
139 efficiency. The MFWAM model is used for the global wave system of the Copernicus Marine
140 Service with a recent update which takes into account a spectra tail in the form of the Phillips'
141 spectrum. This parameterization is important for the calculation of the total stress provided to the
142 ocean model and the impact of waves on the atmosphere in a coupled simulation.

143 In the present study the model MFWAM uses a discretization of the wave spectrum in 24
144 directions (from 0 to 360°) and 30 frequencies increasing from 0.035Hz with a geometric
145 progression of 1.1. The MFWAM model is set for a global configuration with a grid resolution of
146 0.5°. The model is forced by analyzed winds and sea ice fraction provided by the IFS
147 atmospheric system of the ECMWF. Four sets of simulations were run : (i) with assimilation of
148 wavenumber components K_x and K_y from SWIM spectra (run A); (ii) with assimilation of
149 SWIM SWH only (run B); (iii) with assimilation of both SWH and wave number components

150 (run C); and (iv) without assimilation (run D) as a control run to examine the impact (or to build
151 a benchmark database).

152 Wavenumber components were assimilated into the model with the following scheme
153 (Aouf et al., 2006 & 2019): (i) model and SWIM spectra are partitioned to separate wind sea
154 from swell systems, following Gerling (1992); (ii) partitions of the model spectra are matched
155 with the SWIM counterpart; (iii) an optimal interpolation between model and observations to the
156 two components K_x and K_y of the partition wave number is applied; and (iv) analyzed partitions
157 are superposed to reconstruct the analyzed wave spectrum, with smoothing procedure to avoid
158 gaps between partitions. Only modes with wavelengths greater than 70 m were used for the
159 assimilation, while the first guess wave spectrum from the model stays unchanged otherwise.

160 The assimilation of SWH from SWIM instrument at nadir look consists in performing only the
161 optimal interpolation scheme for SWH (as a stand-alone procedure or in conjunction with the
162 assimilation of wavenumber components). Note, however, that assimilation of SWH further
163 requires a scaling of the wave spectrum in the frequency range by using the empirical power
164 laws developed in Lionello et al. (1992). This is the classical approach as used in most
165 operational models (see Aouf and Lefevre 2015).

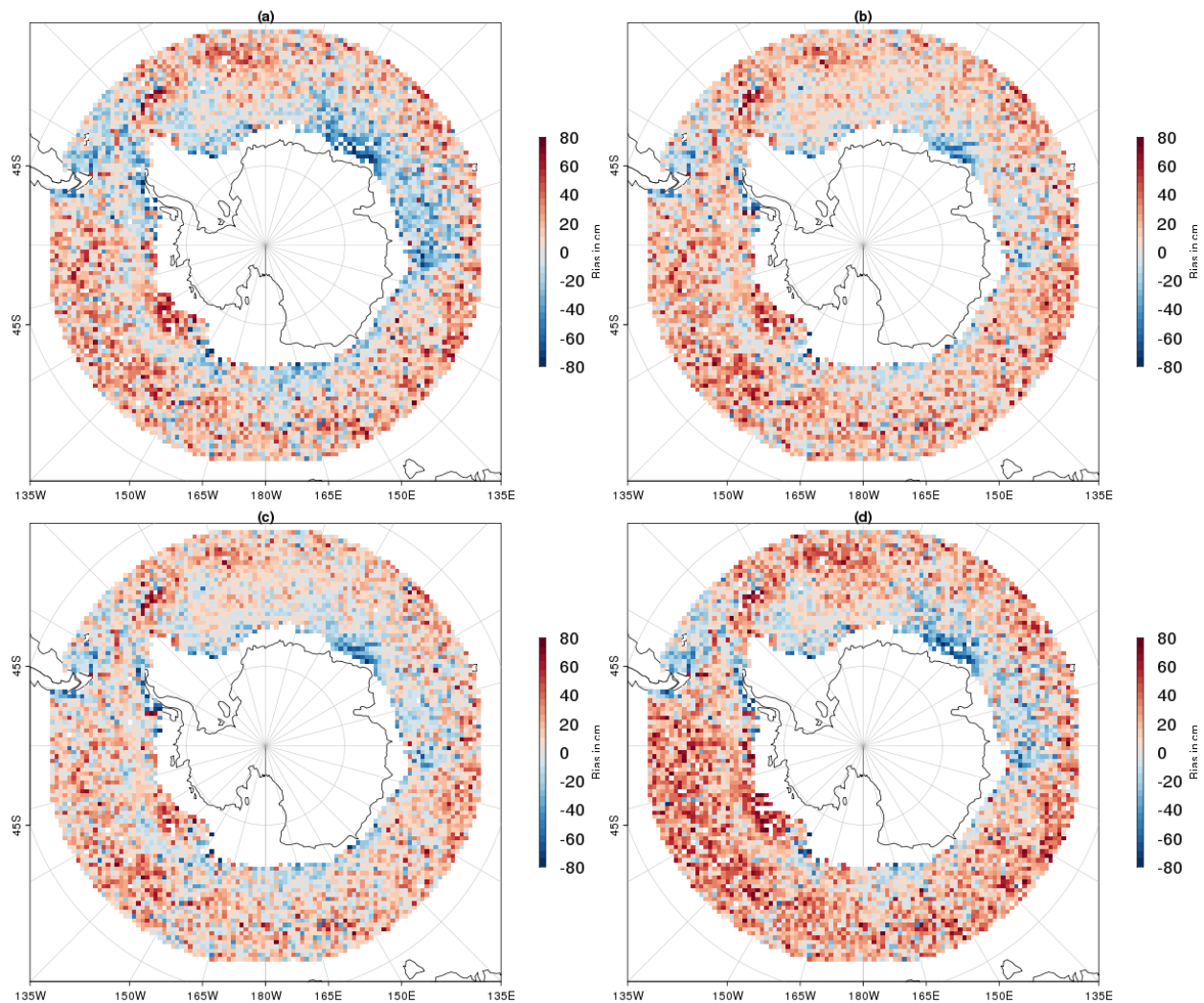
166 The study area focuses on the Southern Ocean where a large number of storm events with strong
167 winds are generated during the Southern winter. We should remark that during the period of
168 study surface wind speed exceeding 20 m/s represent 30% for the Pacific Southern Ocean
169 between the longitudes 150°E-250°E.

170 The Southern Ocean is well covered by altimeter missions. Therefore, the validation of
171 the model simulations is based on significant wave heights provided by the Jason-3, Saral/Altika
172 and Sentinel-3 altimetry missions in this region. Super-observations of SWH from altimeters
173 have been generated on the grid size of the model, which is $0.5^\circ \times 0.5^\circ$. Thus, to evaluate the
174 impact of assimilation, we compare SWH from the four model runs with those provided by the
175 altimeters on this grid size.
176

177 **3 Results and discussions**

178 Biases on SWH from the model runs, with respect to the independent altimeter data, are
179 presented in Fig.1 as maps covering the $[50^\circ\text{S} - 70^\circ\text{S}]$ area. For all runs, we can clearly see a
180 dominant trend of positive bias in the Southern Ocean and the highest values are often found in
181 the Pacific Southern Ocean. However negative bias of SWH are also observed in the Atlantic and
182 Indian ocean near the Marginal Ice Zone (MIZ), where it is expected a strong uncertainty on
183 local winds related to sea-ice melt-water. There is an evident reduction of bias when assimilating
184 satellite data into the model. On average, the control run (without assimilation) leads to a mean
185 bias for SWH of approximately 0.13 m (Fig. 1d) with maximum values reaching 1 m. The mean
186 bias reduces to 0.10 m when assimilating the SWH (Fig. 1b). Incorporating wavenumbers in the
187 assimilation contributes significantly to reduce the bias, the latter dropping to 0.03 m for
188 assimilation of wavenumbers only (Fig. 1c) and 0.05 m, when assimilating both wavenumbers
189 and SWH (Fig. 1c).

190 To examine the impact of the assimilation on high SWH in Southern Ocean, scatter analysis of
191 SWH from MFWAM versus the one from altimeter sensors have been performed for SWH
192 greater than 5 m. Overall, run A results in an excellent correlation with altimeter data, with
193 scatter diagram laying on the slope 1:1 and intercept of 0.04m, substantiating the significant bias
194 reduction. On the contrary, run B shows an overestimation of model results, with data point
195 distributing along a slope of 1.05 and intercept of -0.19m and a mean positive bias of 0.13 m. In
196 terms of Normalized Root Mean Square Error (NRMSE), the best performance for high SWH
197 (greater than 5m) is obtained when assimilating wavenumber components (runs A and C) with
198 10.3%. While for the assimilation of SWH only and the control run, NRMSE are roughly 10.6%
199 and 11%, respectively.

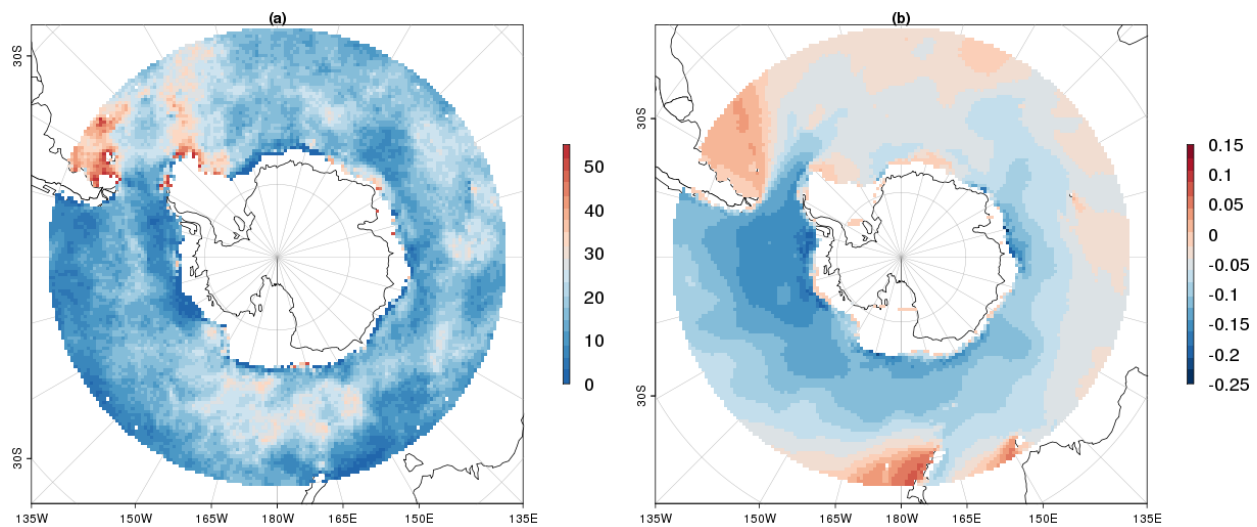


200
201 **Figure 1.** Bias maps of SWH (in cm) for simulations of the MFWAM model in comparison with
202 altimeters Jason-3, Saral/Altika and Sentinel-3 during the period starting from 26 April to 1 June
203 2019. (a), (b), (c) and (d) indicate runs A, B, C and C, respectively.

204 To explain this finding, it is interesting to note that in the wind wave growth phase there is a
205 transfer of wave energy from the high frequencies to the smaller frequencies until an equilibrium

206 state is reached. In general the wind input term in a wave model which describes the wave
207 growth depends, for each frequency, upon the difference of wave and wind directions. The fact
208 that the assimilation of wavenumber components corrects the wave direction and the dominant
209 frequency leads directly to an improvement of the wave growth and the energy transfer for wind
210 waves before the equilibrium state.

211 Recall that the wave age which is expressed as the ratio of peak wave phase speed C_p and the
212 surface wind speed U_{10} , indicates whether the sea state is windsea or swell dominant. The
213 windsea can therefore be identified by a wave age C_p/U_{10} lower than 1. Figure 2a shows the
214 regional distribution of wind sea, by the probability of occurrence associated with a wave age
215 smaller than 1 (estimated over the analyzed period). There is a general predominance of wind sea
216 throughout the entire Atlantic Ocean and Indian Ocean sectors. This is due to the occurrence of
217 relatively close storm systems, which limits fetch for wave growth.

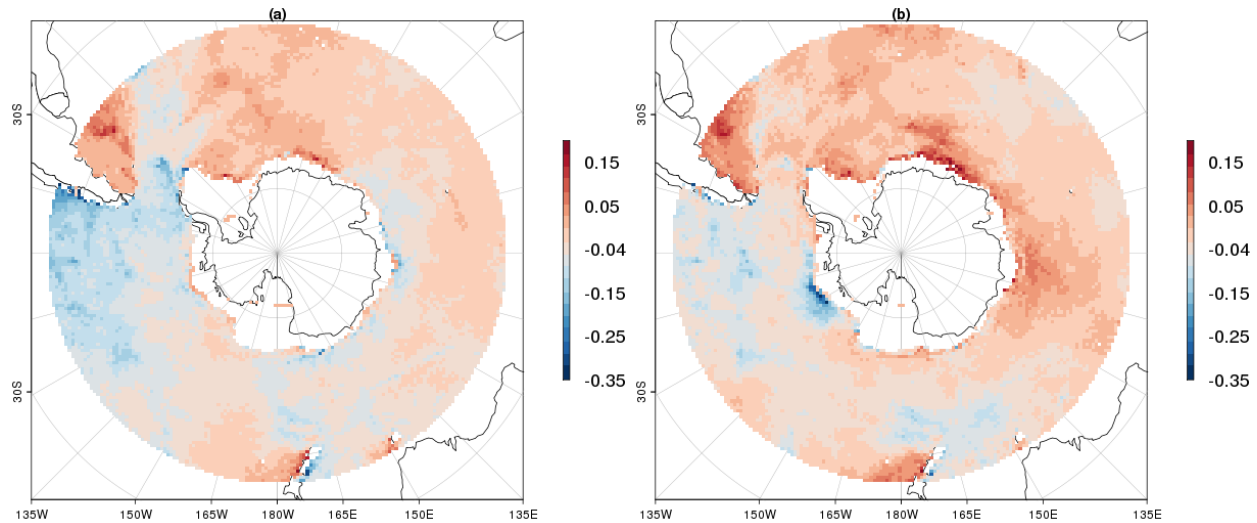


218
219 **Figure 2.** (a) Probability of occurrence (color code) of dominant windsea sea state
220 ($C_p/U_{10} < 1$) from the control run A. (b) mean difference of SWH between run A and run D during
221 the period from 26 April to 1 June 2019.

222 The Pacific Ocean sector, on the contrary, shows two distinct occurrence zones. The first
223 zone is an extended area between 150°E-150°W and South of New Zealand representing a strong
224 occurrence (greater than 25%) of wind sea with uninterrupted fetch conditions. Elsewhere of this
225 zone the low probability of wind sea (i.e. predominance of swell) indicate the presence of fully-
226 developed waves of swell, for instance the drake passage and Chile sector. Figure 2b shows the
227 difference between the mean SWH derived from model runs with assimilation of partition
228 wavenumber components (run A) and benchmark simulation (run D). The assimilation results in
229 a significant reduction of the significant wave height throughout the Southern Ocean in
230 comparison with the control run. The extent of this difference depends on the wave age (cf.
231 Figure 2a). Small differences are reported in the Atlantic Ocean and Indian Ocean Sector, where
232 swell is not dominant (cf. Fig. 2a), while the largest average differences—up to -0.25 m—are
233 found in the Pacific Ocean sector, especially in the Amundsen Sea and Bellingshausen Sea

234 subsectors and in the Drake passage. There are the areas where the wind sea generated South of
235 New Zealand has transformed into a swell after a long, uninterrupted propagation.

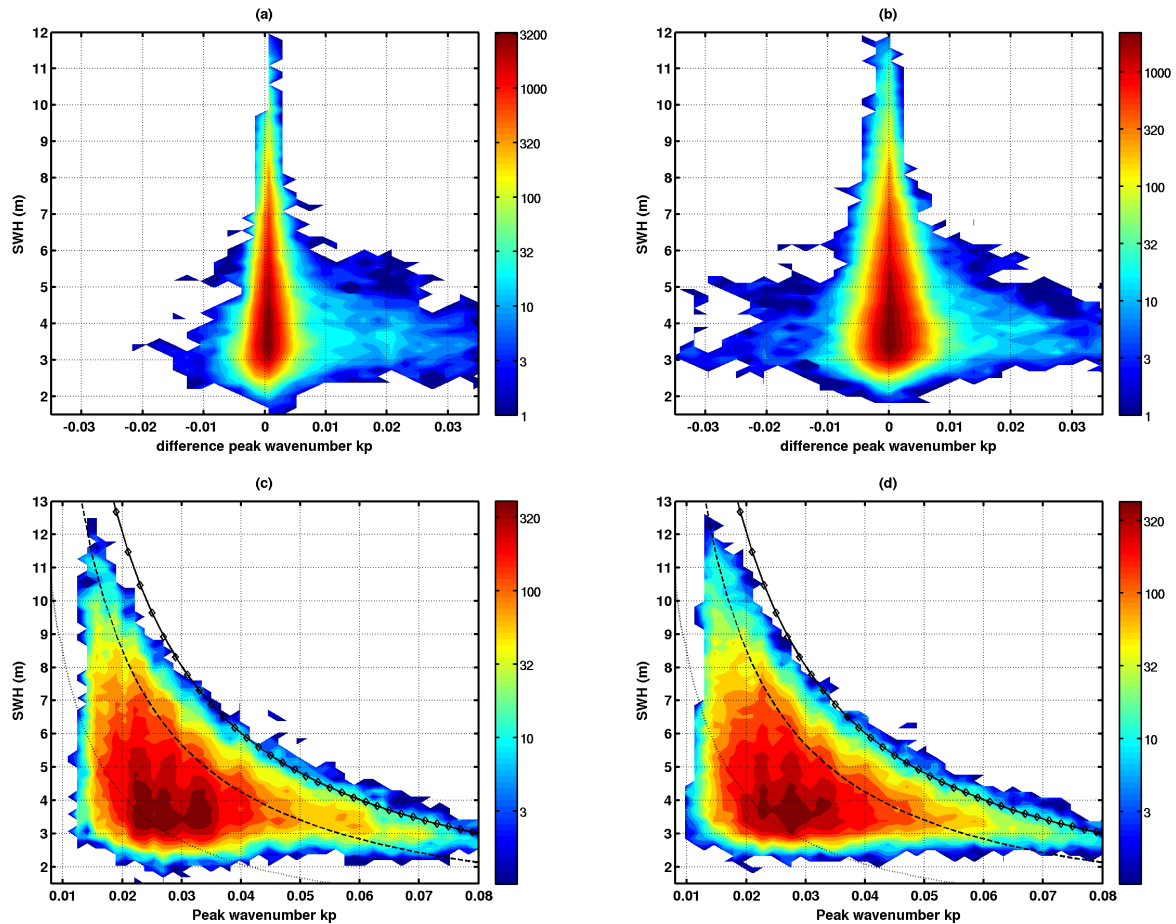
236 Let's call the difference between assimilation runs and the control run the analysis
237 increment. The impact of run A on the peak wave age indicates two trends on the analysis
238 increment as shown in Figure 3a. The first trend concerns the Pacific Ocean sector and Drake
239 Passage where there is a strong negative analysis increment on average which is linked to the
240 overestimation of the wave age by the run D. The average difference in this sector reaches -0.25.
241 The second trend is observed in the Atlantic and Indian oceans sectors where we see that the
242 assimilation of partitions wavenumbers induces a positive increment. This latter indicates an
243 underestimation of the wave age by the control run D with a maximum average difference of
244 0.15. By comparing figures 3a and 3b we see that run B mainly indicates positive increments in
245 all sectors and enhanced in some regions the impact in comparison with run A. The negative
246 increment caused by run B is limited and not significant correction. This can be explained by the
247 use of empirical power laws (Lionello et al. 1992) which seems less efficient to correct peak
248 wave age in unlimited fetch conditions in Pacific Southern Ocean.



249
250 **Figure 3.** Average of difference of wave age (C_p/U_{10}) of runs with and without assimilation
251 during the period between 26 April and 1 June 2019. (a) stand for the assimilation of
252 wavenumber components (run A), while (b) indicate the assimilation of SWH only. Negative
253 values mean overestimation of wave age and conversely positive values indicate underestimation
254 of the control run.

255 To investigate the difference between run A and run B we analyzed the analysis
256 increment of dominant wavenumbers from these two runs in comparison with the control run D.
257 Figure 4a and 4b show respectively the analysis increment of the dominant wavenumber of runs
258 A and B as a function of SWH located on the altimeters tracks used for the bias evaluation in the
259 Southern Ocean. We can clearly see that the assimilation of the partition wavenumbers mainly
260 leads to a positive correction of the dominant wavenumber k_p (Fig.4a), which indicates an
261 underestimation of the control run D. This increase of the wave number is clearly visible for
262 strong SWH (greater than 5 m), which shows that assimilation maintains the wave regime in the

263 growth phase. Figure 4c reveals that the majority of the dominant wavenumbers k_p points are
 264 between the theoretical curves of young and mature seas as given by the Elfouhaily spectrum
 265 (Elfouhaily et al., 1997). Figure 4c clearly indicates a good consistency of the variation of
 266 dominant wavenumber with SWH in comparison with theoretical curves. On the contrary for
 267 run B (Fig. 4b), we notice that the correction of k_p is dominated by negative analysis increments
 268 for strong SWH (greater than 5 m). This explains the difficulty of run B to reduce the bias for
 269 large SWH, and also to improve the dominant wavenumbers during the growth phase. Figure 4d
 270 also indicates that the number of k_p points between the young and mature sea curves is smaller
 271 compared to Figure 4c.



272

273 **Figure 4.**(a,b): variation of analysis increment of peak wavenumber with SWH, for model runs
 274 A and B, respectively. (c,d): Relation between SWH peak wavenumber with, for model runs A
 275 and B., respectively. The dotted, dashed and diamond lines indicate the theoretical variation for
 276 peak wavenumber of young (wave age=0.7), mature (wave age=1) and fully developed (wave
 277 age=1.2) seas according to the wave spectrum model of Elfouhaily et al. (1997). With equations
 278 (37) and (38) in Elfouhaily et al.(1997), we obtained the following relation $SWH=(0.17/k_p)*\Omega^{-1.7}$
 279 where Ω is the inverse wave age. Color bars indicate the density of points by pixel.

280 **4 Conclusions**

281 The Southern Ocean is dominated by strong wave systems which can impact air-sea
282 interaction and ocean and sea-ice dynamics (e.g. Humphries et al. 2016; Schamle et al. 2019,
283 Thurnherr et al. 2020, Vichi et al. 2019, Alberello et al. 2020). Contemporary wave models
284 provide biased estimates of the significant wave height in this region, despite assimilation of
285 satellite observations. These, however, are limited to significant wave height or truncated
286 directional wave energy spectra, which account for swell systems, but neglect the short wave
287 components of the wind sea. However, with the instrument SWIM carried by the CFOSAT
288 satellite, it is now possible to detect directional wave spectra that resolve both swell and wind-
289 wave systems. This study has demonstrated that the assimilation of the wavenumber components
290 from more comprehensive spectra enhance model prediction of energy transfer during the wave
291 growth phase and concurrently improve estimation of the significant wave height in the Southern
292 Ocean. A validation was conducted by comparing significant wave height from model runs with
293 and without assimilation against observations from altimeter sensors. Overall, data assimilation
294 reduces biases. Model runs, however, show that assimilation of wavenumber components (i.e.
295 directional properties) is more efficient in optimizing the model and results in more substantial
296 bias reduction (from 13cm bias without assimilation to 3cm with assimilation) than assimilation
297 of significant wave height only.

298 Furthermore, the results show that the assimilation of the wavenumbers components
299 corrects significantly the wave age and the dominant wavenumber in the Southern Ocean, which
300 keeps the wind waves between young and mature seas regimes. This has been verified with the
301 theoretical growth curves (SWH as function with k_p) as given by Elfouhaily et al. (1997). We
302 have observed a better spread of the impact on wave age when using directional observations
303 around the Southern Ocean in comparison with the assimilation of significant wave height only.
304 The transition to swell regime and the propagation in northern ocean region is also well tracked
305 as it is observed in Pacific Southern Ocean. However, the assimilation of SWH only showed a
306 limited and localized impact on the wave age.

307 This research opens perspectives on the use of the directional properties of SWIM
308 instrument of CFOSAT mission to improve wave model and also provide accurate wave spectra.
309 We expect a promising use of the assimilation of wave number components for ocean/waves
310 coupling in terms of momentum flux transfer in southern ocean where gas exchanges are still
311 poorly understood in climate models.

312 **Acknowledgments and data**

313 This work is funded by the French Space Agency CNES in the frame of TOSCA national
314 program. The level 2 data used here are processed by SWIM algorithms version V5.0.1. The data
315 are available and open access on <ftp-access.aviso.altimetry.fr>. The authors would also like to
316 thank Alice Dalphinnet and Malek Ghantous for helping to the preparation of the manuscript.
317

318 **References**

- 319 Alberello, A., Bennetts, L., Heil, P., Eayrs, C., Vichi, M., MacHutchon, K., Onorato, M. &
320 Toffoli, A.: Drift of Pancake Ice Floes in the Winter Antarctic Marginal Ice Zone During Polar
321 Cyclones, *Journal of Geophysical Research: Oceans*, 125, e2019JC015 418,
322 doi.org/10.1029/2019JC015418, 2020.
- 323 Aouf L., Dalphinet, A., Hauser, D., Delaye, L., Tison, C., Chapron, B., Hermozo, L., &Tourain,
324 C. (2019), On the Assimilation of CFOSAT Wave Data in the Wave Model MFWAM :
325 Verification Phase, proceedings of IGARSS 2019 - IEEE International Geoscience and Remote
326 Sensing Symposium, Yokohama, Japan, 2019, pp. 7959-7961, doi:
327 10.1109/IGARSS.2019.8900180.
- 328 Aouf L. & Lefèvre J-M. (2015), On the impact of the assimilation of SARAL/Altika wave data
329 in the operational wave model MFWAM, *Marine Geodesy*, 38, 381-395.
330 doi:10.1080/01490419.2014.1001050
- 331 Aouf, L., Lefèvre, J-M. & Hauser D. (2006), Assimilation of directional wave spectra in the
332 wave modelWAM: An impact study from synthetic observations in preparation for the
333 SWIMSAT Satellite mission. *J Atmos Ocean Technol.* doi: 10.1175/JTECH1861.1
- 334 Ardhuin, F., Rogers, E., Babanin, A., Filippot, J-F., Magne, R., Roland, A., Van Der
335 Westhuysen, A.; Queffeuilou, P., Lefèvre, J-M., Aouf, L. & Collard, F. (2010), Semi empirical
336 Dissipation Source Functions for Ocean Waves. Part I: Definition, Calibration, and Validation. *J.*
337 *Phys. Oceanogr.*, **40**, 1917–1941, doi:10.1175/2010JPO4324.1.
- 338 Babanin A. V., Rogers, E. W., de Camargo, R., Doble, M., Durrant, T., Filchuk, K., Ewans, K.,
339 Hemer, M., Janssen, T., Kelly-Gerrey, B., Machutchon, K., McComb, P., Qiao, F., Schulz, E.,
340 Skvortsov, A., Thomson, J., Vichi, M., Violante-Carvalho, N., Wang, D., Waseda, T., Williams,
341 G. &Young, I. R. (2019) Waves and swells in high wind and extreme fetches, measurements in
342 the Southern Ocean, *Frontiers in Marine Science*, 6, 361, DOI:10.3389/fmars.2019.00361
- 343 Barbariol, F., Benetazzo, A., Bertotti, L., Cavaleri, L., Durrant, T., McComb, P., & Sclavo, M.:
344 Large waves and drifting buoys in theSouthern Ocean, *Ocean Engineering*, 172, 817–828, 2019
- 345 Csanady, G. T.: Air-sea interaction: laws and mechanisms, Cambridge University Press, 2001.
- 346 Collard F., Ardhuin, F. &Chapron, B. :Monitoring and analysis of ocean swell fields from space
347 : New methods for routines observations, *Journal of Geophysical Research*,
348 10.1029/2008JC005215, 14, issue C7, 2005
- 349 ECMWF (2013) Part VII : IFS Documentation CY38R1, Part VII ECMWF Wave Model.
350 <https://www.ecmwf.int/node/9248>
- 351 Ewans K., 1998, Observations of the directional wave spectrum of fetch-limited waves, *J. Phys.*
352 *Oceanogr.*, **28**, 498–512.
- 353 Donelan, M. A., Hamilton, J. &Hui, W. H. (1985) : Directional spectra of wind-generated waves.
354 *Philos. Trans. Roy. Soc. London.*, **A315**, 509–562.
- 355 Elfouhaily, T., Chapron, B., Katsaros, C. &Vandemark, D. :A unified directional spectrum for
356 long and short wind-driven waves. *Journal of Geophysical Research*, Volume 102, C7,
357 <https://doi.org/10.1029/97JC00467>.
- 358 Fadaeiazar, E., Leontini, J., Onorato, M., Waseda, T., Alberello, A.& Toffoli, A.: Fourier
359 amplitude distribution and intermittency in mechanically generated surface gravity waves, *Phys.*
360 *Rev. E*, 102, 013 106, doi.org/10.1103/PhysRevE.102.013106, 2020

- 361 Humphries, R. S., Klekociuk, A. R., Schofield, R., Keywood, M., Ward, J. & Wilson, S. R.:
362 Unexpectedly high ultrafine aerosol concentrations above East Antarctic sea ice, *Atmos.*
363 *Chem. Phys.*, 16, 2185–2206, doi.org/10.5194/acp-16-2185-2016, 2016.
- 364 Gerling, T. W., Partitioning sequences and arrays of directional ocean wave spectra into
365 component wave systems, *J. Atmos. Oceanic Technol.*, 9, 444–458, 1992.
- 366 Hasselmann K., P. T. Barnett, E. Bouws, H. Carlson, E. D. Cartwright, K. Enke, A. J. Ewing, H.
367 Gienapp, E. D. Hasselmann, P. Kruseman, A. Meerburg, P. Muller, D. Olbers, K. Richter, W.
368 Sell, & H. Walden. Measurements of wind-wave growth and swell decay during the joint north
369 sea wave project (jonswap). *Deut. Hydrogr. Z.*, 8 :1–95, 01 1973.
- 370 Hasselmann, D. E. & Dunckel, M. & Ewing, J. A. (1980) : Directional wave spectra observed
371 during JONSWAP 1973. *J. Phys. Oceanogr.*, **10**, 1264–1280.
- 372 Hasselmann K., Chapron B., Aouf L., Ardhuin F., Collard F., Engen G., Heimbach P., Janssen
373 P., Krogstad H., Lehner S., Li J-G., Li Xiaoming, Rosenthal W. & Schulz-Stellenfleth J. (2012) :
374 The ERS SAR Wave Mode – A Breakthrough in global ocean wave observations. European
375 Space Agency, (Special Publication) ESA SP. 1326.
- 376 Hauser D., et al., "New Observations From the SWIM Radar On-Board CFOSAT: Instrument
377 Validation and Ocean Wave Measurement Assessment," in *IEEE Transactions on Geoscience*
378 *and Remote Sensing*, doi: 10.1109/TGRS.2020.2994372.
- 379 Kuik, A. J., van Vledder, G. Ph. & L. H. Holthuisen, (1988): A method for the routine analysis of
380 pitch-and-roll buoy wave data. *J. Phys. Oceanogr.*, **18**, 1020–1034.
- 381 Le Traon P. Y., Reppucci A. & Alvarez Fanjul E. et al (2019) From Observation to Information
382 and Users: The Copernicus Marine Service Perspective. *Front Mar Sci.* doi:
383 10.3389/fmars.2019.00234
- 384 Lionello, P., Gunther, H. & Janssen, P. A. E. M. (1992). Assimilation of altimeter data in a
385 global third generation wave model. *J. Geophys. Res.*, C97, 14453–14474.
- 386 Long, C. E. & Resio, D. (2007). Wind wave spectral observations in Currituck Sound, North
387 Carolina. *J. Geophys. Res.* 112, CO5001.
- 388 Mitsuyasu, H., Tasai, F., Suhara, T., Mizuno, S., Ohkusu, M., Honda, T. & Rikiishi, K. & (1975).
389 Observations of the directional spectrum of ocean waves using a clover leaf buoy. *J. Phys.*
390 *Oceanogr.* 5, 750–760.
- 391 Pierson, W. J., & Moskowitz, L., A proposed spectral form for fully developed wind sea based
392 on the similarity theory of S. A. Kitaigorodskii, *J. Geophys. Res.*, 69, 5181–5190, 1964.
- 393 Phillips, O. M., *The Dynamics of the Upper Ocean*, 2nd ed., Cambridge Univ. Press, New York,
394 1977.
- 395 Resio D. T., Linwood V. & Ardag D., Characteristics of directional wave spectra and
396 implications for detailed-balance wave modeling, *Ocean Modelling*, doi:10.1016/j.ocemod.
397 2015. 09.009
- 398 Schmale, J., Baccarini, A., Thurnherr, I., Henning, S., Efraim, A., Regayre, L., Bolas, C.,
399 Hartmann, M., Welti, A., Lehtipalo, K., Aemisegger, F., Tatzelt, C., Landwehr, S., Modini, R. L.,
400 Tummon, F., Johnson, J. S., Harris, N., Schnaiter, M., Toffoli, A., Derkani, M., Bukowiecki, N.,
401 Stratmann, F., Dommen, J., Baltensperger, U., Wernli, H., Rosenfeld, D., Gysel-Ber, M. &
402 Carslaw, K. S.: Overview of the Antarctic Circumnavigation Expedition: Study of Preindustrial-
403 like Aerosols and Their Climate Effects (ACE-SPACE), *Bull. Am. Meteorol. Soc.*, 100, 2260–
404 2283, doi.org/10.1175/BAMS-D-18-0187.1, 2019.
- 405 Thurnherr, I., Kozachek, A., Graf, P., Weng, Y., Bolshiyarov, D., Landwehr, S., Pfahl, S.,
406 Schmale, J., Sodemann, H., Steen-Larsen, H. C., Toffoli, A., Wernli, H. & Aemisegger, F.:

407 Meridional and vertical variations of the water vapour isotopic composition in the marine
408 boundary layer over the Atlantic and Southern Ocean, *Atmos. Chem. Phys.*, 20, 5811–5835,
409 doi.org/10.5194/acp-20-5811-2020, 2020
410 Toffoli, A., Proment, D., Salman, H., Monbaliu, J., Frascoli, F., Dafilis, M., Stramignoni, E.,
411 Forza, R., Manfrin, M. & Onorato, M., 2017, Wind Generated Rogue Waves in an Annular
412 Wave Flume, *Phys. Rev. Letters*, 118, issue 14, 10.1103/PhysRevLett.118.144503.
413 Toffoli, A., Onorato, M., Bitner-Gregersen, E.M. & Monbaliu, J. (2010). Development of a
414 bimodal structure in ocean wave spectra. *J. Geophys. Res.* 115.
415 Vichi, M., Eayrs, C., Alberello, A., Bekker, A., Bennetts, L., Holland, D., de Jong, E., Joubert,
416 W., MacHutchon, K., Messori, G., Mojica, J. F., Onorato, M., Saunders, C., Skatulla, S. &
417 Toffoli, A.: Effects of an explosive polar cyclone crossing the Antarctic marginal ice zone,
418 *Geophys. Res. Lett.*, 46, 5948–5958, 2019.
419 Young, I. R. 1999: Seasonal variability of the global ocean wind and wave climate, *Int. J.*
420 *Climatol.*, 19, 931-950, doi:10.1002/(SICI)1097-0088(199907)19:9<931
421 Young, I. R., Fontaine, E., Liu, Q., & Babanin, A. V.: The Wave Climate of the Southern Ocean,
422 *J. Phys. Oceanogr.*, 50, 1417–1433, 2020.
423 Young I. R., Verhagen, L. A. & Banner, M. L. (1995) : A note on the bimodal directional
424 spreading of fetch-limited wind waves. *J. Geophys. Res.*, 100 (C1), 773–778.
425 Zieger, S., Babanin, A. V., Rogers, W. E. & Young, I. R.: Observation-based source terms in the
426 third-generation wave model WAVE-WATCH, *Ocean Modelling*, 96, 2–25, 2015.

427

428

429

430

431